Third AO4ELT Conference - Adaptive Optics for Extremely Large Telescopes
Florence, Italy. May 2013
ISBN: 978-88-908876-0-4
DOI: 10.12839/AO4ELT3.13377

WIDE-FIELD WAVEFRONT SENSING IN SOLAR ADAPTIVE OPTICS: MODELING AND EFFECTS ON RECONSTRUCTION

Clémentine Béchet[1,2a], Michel Tallon[1], Iciar Montilla[3], and Maud Langlois[1]

[1] Université de Lyon, Lyon, F-69003, France ; Université Lyon 1, Observatoire de Lyon, 9 avenue Charles André, Saint-Genis Laval, F-69230, France ; CNRS, UMR 5574, Centre de Recherche Astrophysique de Lyon ; Ecole Normale Supérieure de Lyon, Lyon, F-69007, France
[2] Pontificia Universidad Catolica, Astro-engineering department, Santiago, Chile
[3] Instituto Astrofisico de Canarias, Santa Cruz de Tenerife 38205, Spain

Abstract. The planned 4-meter diameter of the European Solar Telescope (EST) is aimed at providing high spatial resolution and large photon collecting area, in order to understand in particular the mechanisms of magnetic coupling in the chromosphere and the photosphere. To reach its goals in the visible and the near-infrared, EST is designed with both a conventional and a multi-conjugate adaptive optics (AO) of similar complexity than the ones featured for the Extremely Large Telescopes. In addition, the AO on EST has to face a particularity of solar AO: the wavefront sensing on extended sources with measurement fields of about 10" in size. Reviewing recent literature together with an independent analysis, we investigate the impact of extended-field sensing in AO for large solar telescopes. Sensing modeling and its effect on reconstruction performance are analyzed, thanks to simulations performed with the Fractal Iterative Method for tomography (FRiM-3D), showing the difficulty to correct high altitude turbulence. We introduce a new approximate direct model of extended-source sensing which greatly improves the quality of the end-to-end simulations for EST AO. Next, we try to improve the conventional solar AO correction by using this new model in the reconstruction. Our simulations do not show significant benefits from using such tomographic model in this conventional AO configuration and under typical atmospheric conditions.

1 Context: the EST adaptive optics

The European Solar Telescope (EST) [1] does not fit in the range of 20 meter-class telescopes, and so is not properly considered as an Extremely Large Telescope (ELT). In fact, it is designed to have a 4 meter-diameter primary mirror, like the Advanced Technology Solar Telescope (ATST) [2] currently under construction. Nevertheless, the solar physics requirements of high Strehl at visible wavelengths and over a wide field-of-view (FOV) with these telescopes lead to the design of adaptive optics (AO) of similar complexity [3] to the ones planned for the ELTs.

The construction of EST is foreseen to start in 2019, in order for the telescope to see its first light in 2025. It is not the scope of this paper to detail neither the high-resolution requirements for EST nor its AO systems, but the main ambitious goals are summarized here [4]. It is expected to have correction abilities over a wide range of elevations down to 15 degrees, as a specific need for solar observations. It is required to provide a corrected FOV of 1 arcmin in diameter with a homogeneous Strehl ratio at 500 nm greater than 30% for r_0 = 7 cm, 50% for r_0 = 14 cm and

[a] CBechetP@ing.puc.cl

60% for $r_0 = 20$ cm. The value of r_0, named Fried parameter, characterizes the strength of the atmospheric turbulence.

The preliminary design of the single-conjugate and multi-conjugate AO for EST has been devised from an analysis of the performances with the evaluation of an error budget and simulations based on Fourier analysis [4]. Their configuration is summarized in Table 1. From

Table 1. Design parameters for EST single-conjugate (SCAO) and multi-conjugate AO (MCAO) [4].

	SCAO	MCAO
# of DMs	1	5
DMs heights (km)	0	0, 2, 6, 10, 23
actuators spacings (cm)	8	8, 30, 30, 30, 30
total # of actuators	$\sim$ 1800	$\sim$ 4000
# of wavefront sensors	1	2
# of sensing fields	1	1, 19
sensing fields size	$10'' \times 10''$	$10'' \times 10''$, $10'' \times 10''$
subaperture size (cm)	8	8, 30
total # of subapertures	$\sim$ 1800	$\sim$ 2000

this preliminary design, end-to-end simulations can henceforth be run in order to accurately assess the AO performance. As a matter of fact, the importance of end-to-end simulations has been previously highlighted [5,6] in studies of large and complex AO systems showing discrepancies with the results of semi-analytic Fourier-based codes. The latter provides erroneous performance prediction in some cases due to the assumption of an infinite size for the sensing aperture. End-to-end simulations have been previously run for the EST [7], but with some approximations due to the use of nighttime AO simulator [8] and reconstruction algorithm [9, 10]. At that time, Octopus, ESO end-to-end AO simulator [8], was chosen for its speed and the diffractive model it uses. Its parallel implementation benefits from a cluster of more than one hundred slaved computers. For the tomographic reconstruction, FRiM-3D algorithm has been chosen [9, 10] for its speed and its low-requirements in precomputations when changing the AO system configurations. These assets of the FRiM-3D are due to its iterative feature, its use of sparse and fast operators and its modeling based on geometric optics.

Nevertheless, Octopus and FRiM-3D were originally designed for nighttime AO and not for solar AO. They did not model the anisoplanatism affecting wide-field wavefront sensing in solar AO. As a first step, it has been decided to upgrade only FRiM-3D, since it can be used both as a simulator and as a reconstruction algorithm. FRiM-3D has thus been adapted to produce more realistic solar end-to-end simulations [11], thanks to the implementation of a wide-field wavefront sensor (WFS) model. The modeling and the analysis of this wide-field sensing in Monte-Carlo simulations for EST is the focus of this paper.

2 Wide-field wavefront sensing impact on AO

Solar AO usually employs Shack-Hartmann wavefront sensors in order to estimate the local gradients over the telescope aperture. The cross-correlation centroiding algorithm has been demonstrated to be a key process in order to close the loops of solar AO systems and make them rather stable [12, 13]. Since it is probing light coming from the sun, it uses wide-field subapertures to

have enough granulation involved in the correlation procedure or to cover the field of interest if it works on a sun spot. On granulation a minimum field of $5'' \times 5''$ is needed, and fields of view larger than $8'' \times 8''$ ensure more robust AO correction [13].

For EST, the conventional AO is planned to use a single high-order WFS of $10'' \times 10''$. The multi-conjugate AO is designed to be a combination of this first AO with a second stage, involving 19 sensed fields of $10'' \times 10''$ low-order WFS leading to a total field of $70'' \times 70''$ [4]. Since the isoplanatic angle at 500 nm is usually smaller than $10''$, the measurement of the turbulence in the upper layers of the atmosphere is affected by anisoplanatism.

2.1 Anisoplanatism model error

This anisoplanatism is usually small and negligible in nighttime AO, because the subapertures, 20 to 50 cm in size, typically look at guide stars in $3'' \times 3''$ fields. Therefore, a narrow-field WFS is usually modeled writing that $x-$slopes d_x^0 follow

$$d_x^0 = \frac{1}{\mathcal{A}} \int_{\mathcal{A}} \frac{\partial}{\partial x} \left(\sum_{l=1}^{n_{\text{layers}}} \phi_l(x, y, 0, 0) \right) dx\, dy = \sum_{l=1}^{n_{\text{layers}}} \frac{1}{\mathcal{A}} \int_{\mathcal{A}} \frac{\partial}{\partial x} \phi_l(x, y, 0, 0)\, dx\, dy\,, \tag{1}$$

where $\phi_l(x, y, 0, 0)$ is the 2D-phase induced by the turbulent layer located at height l, discretized on coordinates (x, y) and in direction of sight $(\theta_x, \theta_y) = (0, 0)$ and $\mathcal{A}$ represents the subaperture area over which the gradient is averaged.

In the case of wide-field sensing, the measurement also includes an averaging of the gradient over the field-of-view $\mathcal{F}$ such that the corresponding x-slopes write

$$\begin{aligned} d_x^{\mathcal{F}} &= \frac{1}{\mathcal{F}} \frac{1}{\mathcal{A}} \int_{\mathcal{F}} \int_{\mathcal{A}} \frac{\partial}{\partial x} \left(\sum_{l=1}^{n_{\text{layers}}} \phi_l(x, y, \theta_x, \theta_y) \right) dx\, dy\, d\theta_x\, d\theta_y \\ &= \sum_{l=1}^{n_{\text{layers}}} \frac{1}{\mathcal{F}} \frac{1}{\mathcal{A}} \int_{\mathcal{F}} \int_{\mathcal{A}} \frac{\partial}{\partial x} \phi_l(x, y, \theta_x, \theta_y)\, dx\, dy\, d\theta_x\, d\theta_y\,. \end{aligned} \tag{2}$$

The last form is just obtained by the linearity of the sum and integrals operators. Using Eqs. (1) and (2), the anisoplanatism contribution to the data can be analyzed as a measurement model error or discrepancy between the narrow-field case and the wide-field sensor. It can thus be evaluated as a quadratic error term associated to each turbulent layer independently

$$< (d_x^{\mathcal{F}} - d_x^0)^2 >_{h_{\text{layer}}} = < \left(\frac{1}{\mathcal{F}} \frac{1}{\mathcal{A}} \int_{\mathcal{F}} \int_{\mathcal{A}} \frac{\partial}{\partial x} (\phi_l(x, y, \theta_x, \theta_y) - \phi_l(x, y, 0, 0)) dx\, dy\, d\theta_x\, d\theta_y \right)^2 >_{h_{\text{layer}}}\,. \tag{3}$$

The anisoplanatism contribution of a given turbulent layer to the data can then be represented by a function of the layer height h_{layer} and r_0 and of the FOV $\mathcal{F}$, as illustrated in Fig. 1. These curves show that for increasing layer height, the averaging is done over a wider area, thus progressively increasing the model error compared to a narrow-field sensing.

2.2 Approximate wide-field model

The FRiM-3D code can use various fast models of Shack-Hartmann sensing both for simulation, but so far no wide-field averaging was included among these models [15]. The narrow-field

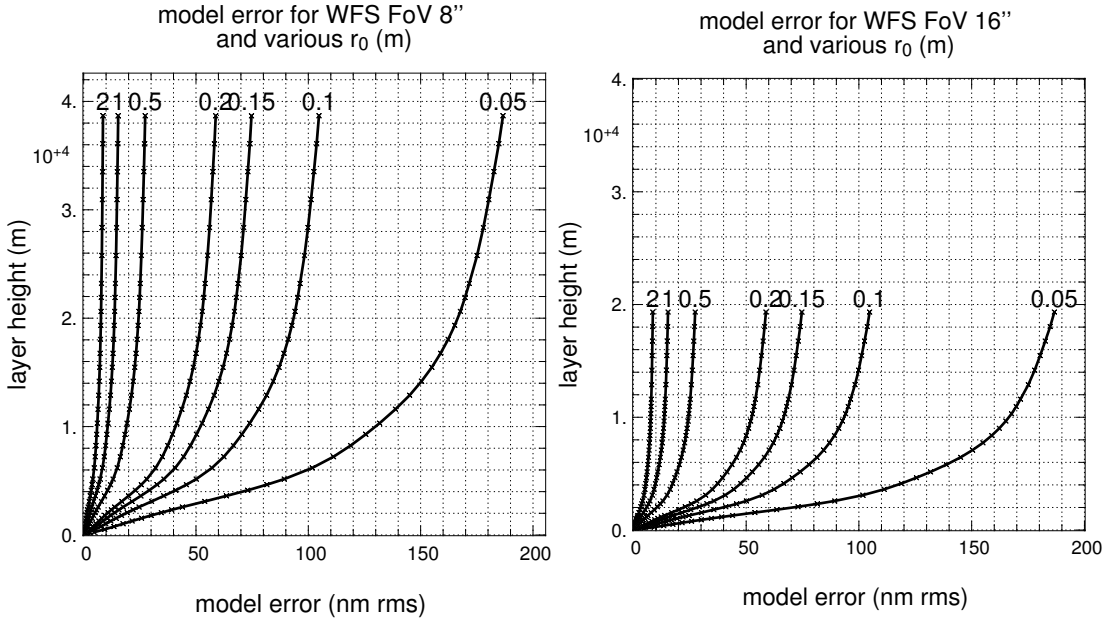

Fig. 1. Modeling error (nm rms) introduced by one turbulent layer at altitude h_{layers} (meters) when WFS fov is 8″ (left) and 16″ (right).The introduced error depends on the value of r_0 in the layer, as represented by the iso-r_0 curves. Curves are plotted for r_0 = 5 cm, 10 cm, 15 cm, 20 cm, 50 cm, 1 m and 2 m.

model in Eq. (1) is implemented and named as *continuous* model. An extension of this *continuous* model for wide-field sensing has been recently implemented, following Eq. (2). The results of the exact representation of the integral over the FOV will be presented in a further communication. Here, we present another model coded in the FRiM-3D, as an approximation of Eq. (2). The field average is replaced by the average of the measurement over $n_{\text{subdir}} = 4$ subdirections in the FOV,

$$d_x^4 = \sum_{i=1}^{n_{\text{subdir}}} \sum_{l=1}^{n_{\text{layers}}} \frac{1}{n_{\text{subdir}}} \frac{1}{\mathcal{A}} \int_{\mathcal{A}} \frac{\partial}{\partial x} \phi_l(x, y, \theta_x(i), \theta_y(i))\, dx\, dy\,, \tag{4}$$

where $\theta_x = [-\theta^{\mathcal{F}}/4, -\theta^{\mathcal{F}}/4, \theta^{\mathcal{F}}/4, \theta^{\mathcal{F}}/4]$ and $\theta_y = [-\theta^{\mathcal{F}}/4, \theta^{\mathcal{F}}/4, -\theta^{\mathcal{F}}/4, \theta^{\mathcal{F}}/4]$ with $\theta^{\mathcal{F}} = 10''$ for a $10'' \times 10''$ FOV for instance. These four directions are taken at half the distance between the center and the corners of the squared FOV. The choice of 4 directions here came from a rough trade-off between computational load and model error.

2.3 Wide-field sensing and EST SCAO performance

The anisoplanatism contribution to the simulated data using this new model must be looked at as an error term, because the WFS model used for wavefront reconstruction do not take into account this effect. Indeed, SCAO wavefront reconstructors with Shack-Hartmann like FRiM-3D are usually based on Eq. (1) or an approximation of it. The left part of Fig. 2 illustrates the contribution of this anisoplanatism to the data for a complete solar SCAO system. Three examples of atmospheric profiles are presented (black, blue, red), with a layer per layer contribution to the error. With a zenith angle $\theta_z = 60$ deg and $r_0 = 15$ cm here, the total anisoplanatism error in the data is of order of 40 nm rms. If one considers a lower elevation, then the same profile will end up with layer heights much larger above the telescope axis and the error contribution of each layer, from Eq. (3), will increase.

The impact of this increasing anisoplanatism error with zenith angle for single-conjugate AO correction has been first enhanced by J. Marino [14] in the context of ATST studies. His results have been reproduced with FRiM-3D simulations on the right part of Fig. 2. The wider the WFS field-of-view or the lower the elevation, the worse the Strehl ratio of the conventional solar AO for EST. Note that the Haleakala profile used here contains most of its turbulence at low altitude, thus showing moderate degradation of the Strehl ratio [14]. The effect is nevertheless significant.

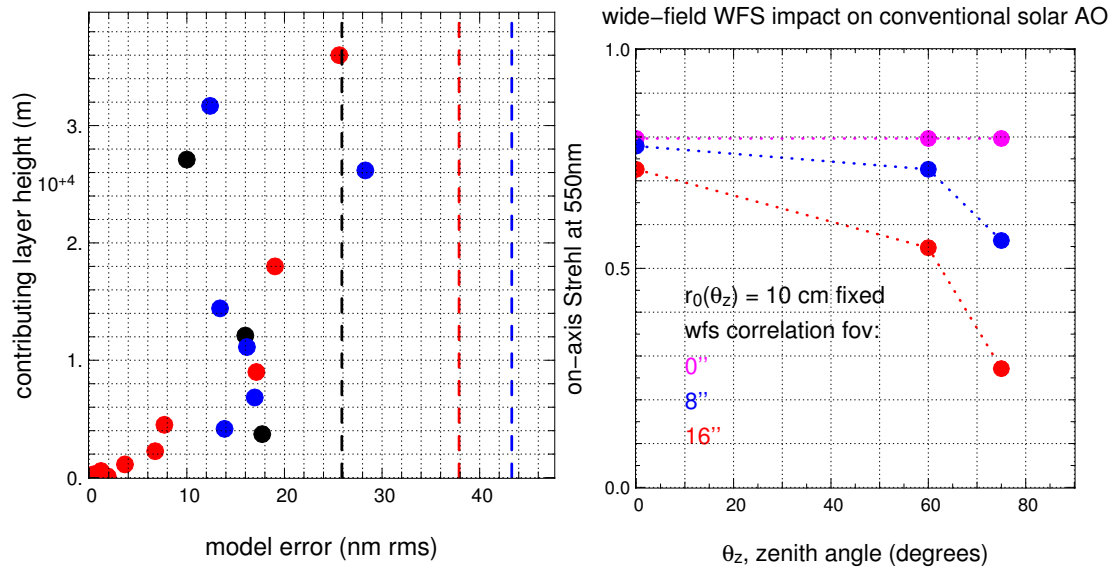

Fig. 2. Left: anisoplanatism contribution to the sensor model error (nm rms) for 8″×8″ FOV, r_0 = 15 cm and θ_z = 60 deg. The contribution of each turbulent layer (colored circles) is independent and add in variance to produce the total anisoplanatism error for a given profile example (dash vertical line in nm rms). Black: Haleakala 3-layer profile from [14]. Blue: Cerro Pachon 6-layer median profile. Red: E-ELT 9-layer median profile used for MAORY phase A study. **Right:** Wide-field WFS impact on conventional solar AO for a 4 meter telescope. The simulations with FRiM-3D use the Haleakala profile from [14]. A constant r_0 of 10 cm is used whatever the zenith angle.

3 FRiM-3D reconstruction with the wide-field model

The results in Fig. 2 show that the anisoplanatism must be simulated in solar AO, in order to predict realistic degradation of the performance of conventional AO at low elevations and to include the relevant anisoplanatism contribution to the data. In the present section, we investigate whether this new wide-field model can also benefit the reconstruction quality.

Changing the atmospheric vertical distribution of turbulence now changes the data when using the wide-field model implemented according to Eq. (4). This new model can also be used for the reconstruction in the algorithm FRiM-3D. Since the input of the direct model can be a set of layers distributed in altitude, the reconstruction with such model can also provide a set of estimated layers distributed at various altitudes. Whereas no tomographic information can be recovered from a single narrow-field WFS, we investigate here whether the use of this new wide-field model could help recovering the vertical distribution of the turbulence.

3.1 Toy case with 1 layer

In a first step, on the left of Fig. 3, we simulate a single turbulent layer in altitude, at three successive heights 6 km, 12 km and 20 km, and we reconstruct it from data of an $8'' \times 8''$ WFS at this same exact height. Both the simulator and the reconstructor use the wide-field model of Sect. 2.2. The reconstruction error inevitably increases with the layer height, revealing the smoothing effect of the averaging over a layer area increasing in size. As a reference, the reconstruction error level for an ideal zero-field WFS is represented with the blue line. It is the minimum error and it is independent of the layer height. Next, the same three cases of single layer are simulated, but the reconstructed layer is assumed to be at a varying height, from 0 to 30 km. The reconstruction error then evolves with this reconstructed layer height as illustrated on the right of Fig. 3, showing that there exists an optimal reconstruction height in each case, approximately where the simulated layer is.

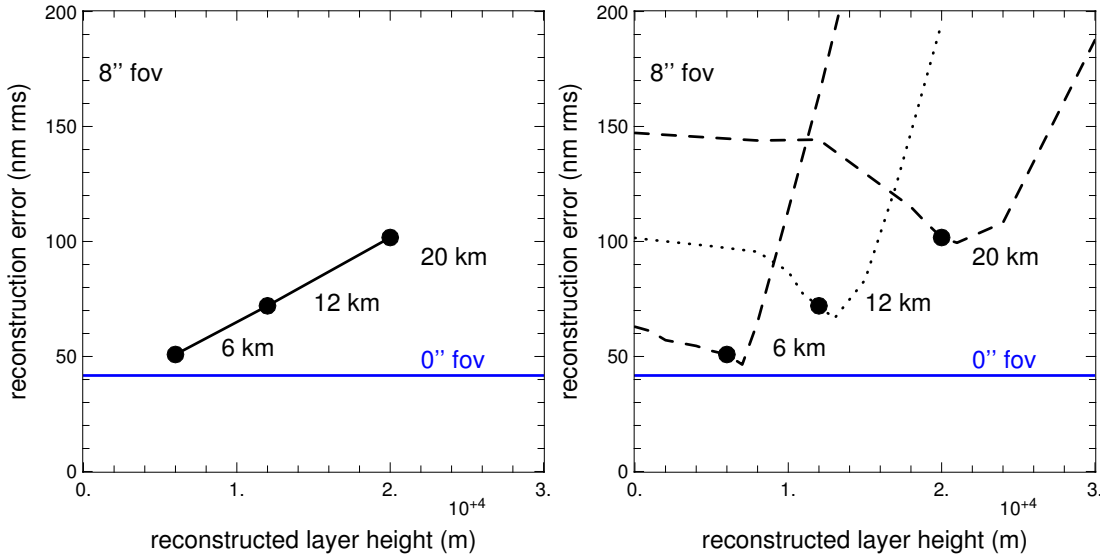

Fig. 3. On-axis error (nm rms) of 1 turbulent layer reconstruction, as a function of the layer height. For a 0-arcsecond fov WFS in blue, and a 8-arcsecond fov WFS in black. $r_0 = 10$ cm for every layer. **Left:** Both simulated and reconstructed layer have the same height. **Right:** 3 cases of reconstructed layers are considered (6km (dash), 12km (dot), and 20km (dash) height), and for each simulated height, the height of the reconstructed layer is tested from 0 to 30 km.

If the reconstruction were made with a conventional narrow-field model, the reconstruction error would always be the value of the dashed and dotted curves for a layer at the ground, on the right of Fig. 3. In other words, the potential reduction of the reconstruction error seems particularly attractive for high layers, with a reduction of ~ 30 nm rms for 12 km, and ~ 50 nm rms for the layer at 20 km.

3.2 Toy case with 2 layers

In a second step, we test if the tomographic reconstruction with the new wide-field WFS model is able to distinguish between contributions of two different altitudes. A single layer is simulated in altitude but the algorithm is applied to reconstruct two layers: one at the ground and the other one at a varying height (from 0 to 30 km in abscissae on left of Fig. 4). The FRiM-3D

reconstruction method requires to set *a priori* values for the C_n^2 distribution between the 2 layers. If these priors are set to 50% on the ground and 50% in altitude, the black dashed and dotted curves in Fig. 4 are obtained. It is necessary to set the priors to 1% on the ground and 99% on the altitude layer in order to recover 2 reconstructed layers with almost all the turbulence well attributed to the highest layer, as shown in red on the left of Fig. 4. The correct priors on C_n^2 are crucial to reconstruct the turbulence at the correct altitude. This means that the tomography is highly degenerated and the correct attribution of the altitude mainly relies on the priors values.

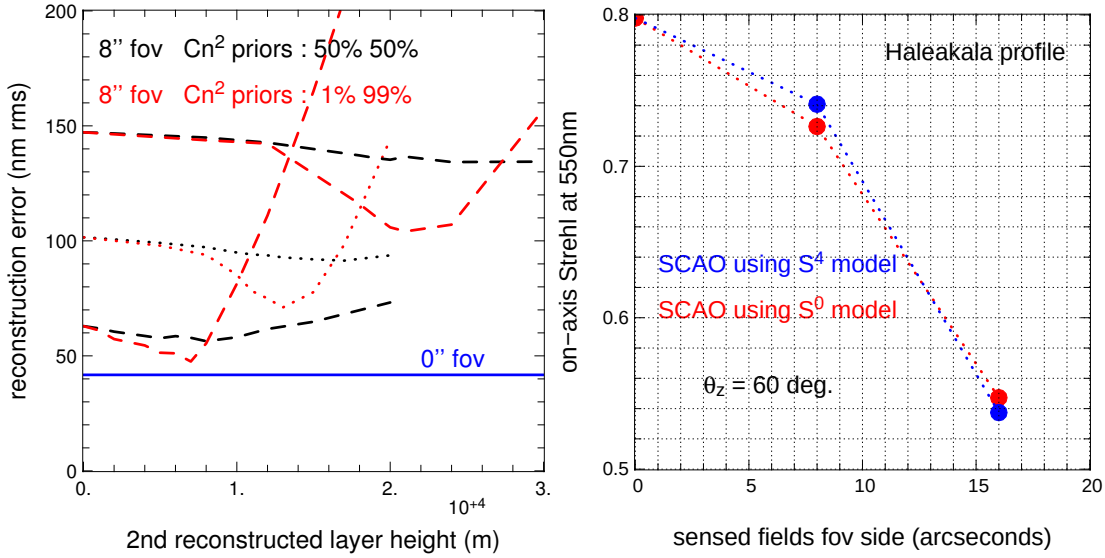

Fig. 4. Left: On-axis error (nm rms) of 1 turbulent layer simulation with 2 reconstructed layers in the model (one on the ground and one at height mentioned on x-axis), as a function of the simulated layer height. For a 0-arcsecond fov WFS in blue, and a 8-arcsecond fov WFS in black and red. $r_0 = 10$ cm. 3 cases of simulated layer are considered (6km (dash), 12km (dot), and 20km (dash) height), and for each simulated height, the height of the recosntructed layer is tested from 0 to 30 km. Black: C_n^2 priors are $50\% - 50\%$. Red: C_n^2 priors are $1\% - 99\%$.**Right:** Comparison of SCAO performance on EST with (blue) or without (red) the wide-field model reconstruction, for increasing WFS field of view (0″, 8″ and 16″).

3.3 Complete atmosphere tomography

Despite the possibility of the wide-field sensor model in FRiM-3D to reconstruct layers at different heights, the correct distribution of the reconstructed turbulence in altitude seem from the left of Fig. 4 to mainly rely on the priors validity. As a last test, a complete Haleakala turbulence profile has been simulated and the reconstruction with the narrow-field model and the one with the wide-field model are compared on the right of Fig. 4. The FRiM-3D reconstruction with the wide-field model (blue) involves exactly the same number and distribution of layers as the simulated profile. The exact prior values for the C_n^2 are also used. Nevertheless, the wide-field model does not reveal any significant improvement of the correction, compared to a narrow-field one.

Similar results have been obtained with other simulated profiles, elevations, seeing conditions and noise level. There is no quantitative benefit of the wide-field model for single-sensor reconstruction. This means that the average of the data over the wide-field of view definitely degrade the possible SCAO correction. The impact of this new model on tomographic AO is however still an open question, tackled with preliminary results in Montilla *et al.* [11].

4 Conclusion and Future work

The European Solar Telescope will feature a challenging adaptive optics (AO), combining single-conjugate and multi-conjugate AO. End-to-end simulations have been run in collaboration between the CRAL (France) and the IAC (Spain). This is aimed at consolidating the error budget of this complex AO, including 5 deformable mirrors and a combination of low-order and high-order sensing. It is also the opportunity to investigate specific issues of solar AO like the anisoplanatism effect for conventional AO treated in this paper.

The FRiM-3D simulator and reconstructor have been upgraded to model the anisoplanatism effect in solar wide-field sensing. This effect is shown to introduce an error in the data ranging from a few nm rms to about 100 nm rms. The introduction of this wide-field model in the simulator allows to produce more realistic performance evaluations. In particular, this is foreseen to be used for simulations of EST and Big Bear Solar Observatory MCAO systems.

Finally, the use of a wide-field model for reconstruction does not significantly improve the AO correction for SCAO, compared to the use of a narrow-field sensing model. The drop of the performance of conventional solar AO for telescopes of 4-meter diameter cannot be compensated for with a more accurate modeling. This highlights the noxious effect of the high altitude data averaging due to the wide sensed fields.

References

1. M. Collados, F. Bettonvil, L. Cavaller, I. Ermolli, B. Gelly, A. Pérez, H. Socas-Navarro, D. Soltau, R. Volkmer *et al.*, Astronomische Nachrichten **331** (2010), pp.615–619.
2. S. Keil, T. Rimmele, and J. Wagner, Earth, Moon, and Planets **104** (2009), pp.77–82.
3. M. Collados, Lecture Notes and Essays in Astrophysics **3** (2008), pp. 113–130.
4. T. Berkefeld and D. Soltau, Astronomische Nachrichten **331** (2010), pp. 640.
5. A. G. Basden, N. A. Bharmal, R. M. Myers, S. L. Morris, and T. J. Morris, Mon. Not. R. Astron. Soc., **435** (2013), pp. 992-998.
6. M. Le Louarn, R. Clare, C. Béchet, and M. Tallon, *Proc. SPIE, Adaptive Optics Systems III* **8447** (2012).
7. I. Montilla, C. Béchet, M. Le Louarn, M. Tallon, J. Sánchez-Capuchino, and M. Collados Vera, *Proc. SPIE, Adaptive Optics Systems III* **8447** (2012).
8. M. Le Louarn, C. Verinaud, and V. Korkiakoski, Comptes Rendus Physique **6** (2005), pp. 1070-1080.
9. E. Thiébaut and M. Tallon, J. Opt. Soc. Am. A **27** (2010), pp. 1046-1059.
10. M. Tallon, I. Tallon-Bosc, C. Béchet, F. Momey, M. Fradin, and É. Thiébaut, *Proc. SPIE, Adaptive Optics Systems II* **7736** (2010), pp. 77360X.
11. I. Montilla, C. Béchet, M. Langlois, M. Tallon, M. Collados, *AO4ELT3 Conference Proceedings*, **13272** (2013).
12. O. von der Luehe, Lecture Notes in Physics, Berlin Springer Verlag **233**(1985), pp. 62-82.
13. T. R. Rimmele and J. Marino, Living Reviews in Solar Physics **8** (2011).
14. J. Marino, Optical Engineering **51** (2012), pp. 101709.
15. F. Momey and M. Tallon, *1rst AO4ELT Conference Proceedings*, **03009** (2010).
16. M. Langlois, G. Moretto, C. Béchet, I. Montilla, M. Tallon, P. Goode, N. Gorceix and S. Shumko *AO4ELT3 Conference Proceedings*, **13316** (2013).